Journal of Applied Electrochemistry **29**: 661–669, 1999.

Gas evolution and power performance in direct methanol fuel cells

P. ARGYROPOULOS, K. SCOTT* and W.M. TAAMA
Department of Chemical and Process Engineering, University of Newcastle upon Tyne, Newcastle upon Tyne NE1 7RU, Great Britain
*(*author for correspondence)*

Received 13 July 1998; accepted in revised form 11 November 1998

Key words: direct methanol, flow visualization, fuel cell, gas liquid, solid polymer electrolyte

Abstract

The use of acrylic cells and a CCTV camera for visually investigating the carbon dioxide gas evolution process inside an operating direct methanol fuel cell environment is demonstrated. Also, the effect of operating parameters on the system gas management, using a series of tests with different gas diffusion layer supporting materials, flow bed designs, cell sizes and exhaust manifold configurations, is studied. Carbon dioxide gas management is an important issue obstructing progress in viable direct methanol fuel cell systems development. Gas evolution mechanisms and gas management techniques are discussed and analysed with reference to several video picture and performance data. The data demonstrate that Toray carbon paper is not a suitable material for DMFCs due to its poor gas removal properties. 'A' type carbon cloth shows relatively good gas removal behaviour. Increasing the liquid phase inlet flow rate is beneficial for gas removal. Increasing the current density results in higher gas production and in the formation of gas slugs, especially at low flow rates, which can lead to blocking of the channels and hence deterioration in the cell performance. A new flow bed design, based on a heat exchanger concept, is affective for gas management and gives a more uniform flow distribution in the flow bed channels. Using the results of this study, and the modelling techniques developed by our group, will are able to determine suitable operating conditions for our prototype 0.5 kW cell DMFC stack.

1. Introduction

The direct methanol fuel cell (DMFC) is a promising power source for transportation and portable power. A great deal of research has recently focused on the direct methanol fuel cell (DMFC) based on solid polymer electrolyte membranes (e.g., [1–9]). A number of groups have reported performance data for liquid feed DMFCs (e.g., Ravikumar and Shukla [3], Surampudi et al. [4], Valdez et al. [5] and Narayanan [6]). Surampudi et al. [4], reported the performance of a DMFC with solid polymer electrolyte (Nafion®) using a supported Pt/Ru catalyst anode of unknown manufacture. The influence of temperature and methanol concentration was briefly reported. The performance of a small stack of five cells (25 cm^2 cross section) at temperatures of less than 60 °C has been reported [5]. The catalyst loading was 4 mg cm^{-2} of an in house Pt/Ru catalyst supported on carbon. Power densities between approximately 150 to 300 mW cm^{-2} have been reported for liquid feed DMFC using different fabrication procedures (mainly undisclosed) [6]. In addition a membrane material (unidentified) with a significantly reduced crossover of methanol in comparison to Nafion® 117 is reported. A liquid feed DMFC with power output of 0.2 W cm^{-2} at an operational temperature of 95 °C and 4 bar oxygen pressure has been reported by Ravikumar and Shukla [3]. Catalyst loading used were 5 mg cm^{-2} on either electrode. The optimized methanol concentration that could be used, without significant methanol cross-over from the anode to the cathode, is 2 mol dm^{-3}. Electrochemical losses at both electrodes in the DMFC lead to a significant reduction in overall performance, from the theoretical thermodynamic maximum, and thus a focus of research is to minimize these losses through the use of new proton conducting membranes with reduced methanol permeability but with high conductivity, new anode catalysts and structures, new cathode catalyst tolerable to the presence of methanol and new MEA fabrication procedures.

The DMFC consists of a solid polymer electrolyte membrane (proton conducting) onto either side of which are attached catalyst layers comprising typically of platinum (for cathode) or platinum/ruthenium (for anode) catalysts supported, or not, on high surface area carbon and bonded with Nafion® and/or Teflon. The catalyst layers are then covered by gas diffusion layers (typically graphite cloth or paper) to form the membrane electrode assembly (MEA). This assembly is then sandwiched between graphite blocks which have flow beds machined into the surface for the supply of fuel and oxidant and which enable electrical connection to the cell.

The reaction that occurs at the DMFC anode is

$$CH_3OH + H_2O = 6\,e^- + 6\,H^+ + CO_2$$

Carbon dioxide is a reaction product that should be removed from the electrode structure and cell as efficiently as possible. The presence of relatively large amounts of carbon dioxide reduces the free area for the flow and inhibits, to a great extent, the penetration of reactants to the catalyst layer. This last phenomenon is affected by high gas residence time inside the cell, which can entrap gas inside the gas diffusion layer and thus block the microchannels in that structure. This blocking may impede the flow of methanol reactant to the anode catalyst and limit the extent of oxidation or cause a concentration polarization at the anode, which reduces the cell voltage. The problems of carbon dioxide gas management, gas release from the interior of the membrane electrode assembly to the flow bed channels, and efficient gas removal from the cell to the exhaust manifold, are extremely significant with large cell stacks. This scale up procedure overall is complex, since certain phenomena that take place inside an operating cell have not yet been investigated.

To investigate gas management and flow, we have used transparent acrylic DMFCs, which enable the gas evolution and two-phase flow to be observed in the anode flow channel. A number of parameters were investigated in this study: two flow bed designs, two cell sizes, two gas diffusion layer materials, and the effect of liquid inlet flow rate and operating current density.

2. Experimental details

The MEAs were prepared according to previously published procedures [1,9]. Briefly the anode consisted of a Teflonised carbon support (E-Tek, type 'A' or Torray carbon paper), upon which was spread a thin layer of uncatalysed (ketjenblack 600) carbon, bound with 10 wt % Nafion® from a solution of 5 wt % Nafion® dissolved in a mixture of water and lower aliphatic alcohol's (Aldrich). The catalysed layer, Pt–Ru dispersed on carbon (2 mg cm^{-2} metal loading) and bound with 10 wt % Nafion®, was spread on this diffusion backing layer. The cathode was constructed using a similar method as for the anode, a diffusion layer bound with 10 wt % PTFE and a catalyst layer consisting of 10 wt % Pt on carbon catalyst with a loading 1 mg cm^{-2} Pt black (Johnson Matthey) with 10 wt % Nafion®. The electrodes were placed either side of a pretreated Nafion® 117 membrane (Aldrich). A thin layer of Nafion® solution was spread onto the surface of each electrode. The MEA was obtained by hot pressing the anode and cathode on either side of the pretreated membrane. The Pt–Ru anode catalyst was 35 wt % Pt, 15 wt % Ru (Johnson Matthey Technology Centre development material).

The characteristics of the carbon cloth and carbon paper are, respectively, as follows: (a) Carbon cloth, density 0.33 g cm^{-3}, porosity 0.85, thickness 0.36 mm, 20% Teflon content, and (b) carbon paper, density 0.49 g cm^{-3}, porosity 0.77, thickness 0.36 mm, 20% Teflon content.

Figure 1 shows a magnified image of the surface of the carbon cloth and carbon paper where the differences in

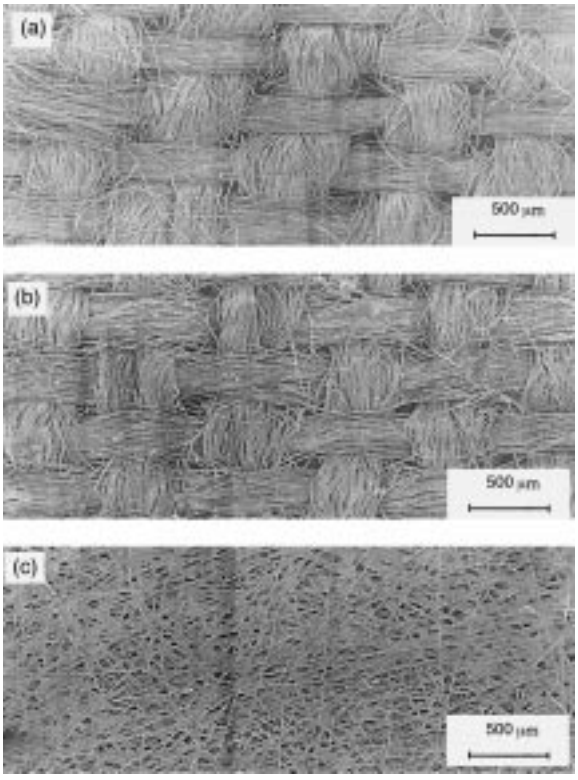

Fig. 1. Photographs of the surfaces of the carbon cloth and carbon paper backing layers. Scalebars 500 μm. (a) Unteflonized E-TEK type A carbon cloth; (b) 20 wt % teflonized E-TEK type A carbon cloth; (c) 20 wt % teflonized E-TEK Toray carbon paper.

the surface morphology are readily apparent. The paper has a structure with a pore size between 20 to 50 μm but has a large proportion of blocked passages. The cloth weave produces a series of relatively large openings, approximately 50 to 100 μm in size, with a Teflonized mat area with smaller openings. The former channels presumably act as liquid flow channels while the latter act predominantly as gas flow channels.

Figure 2 shows the two cell designs investigated in this study. These comprise a small scale cell with an active cross-sectional area of 9 cm^2 and a larger cell with an active cross-sectional area of 102 cm^2. The cells used were made from transparent acrylic, for the anode side, and from graphite block, for the cathode side. The small cell had a set of ten parallel flow channels, 2 mm deep, 2 mm wide and 30 mm long machined into the acrylic block. The width of the ribs which formed the flow channels was 1 mm. Flow in and out of the cell was via a series of 2 mm diameter holes at the cell inlet and outlet which connected into a 10 mm diameter internal manifold.

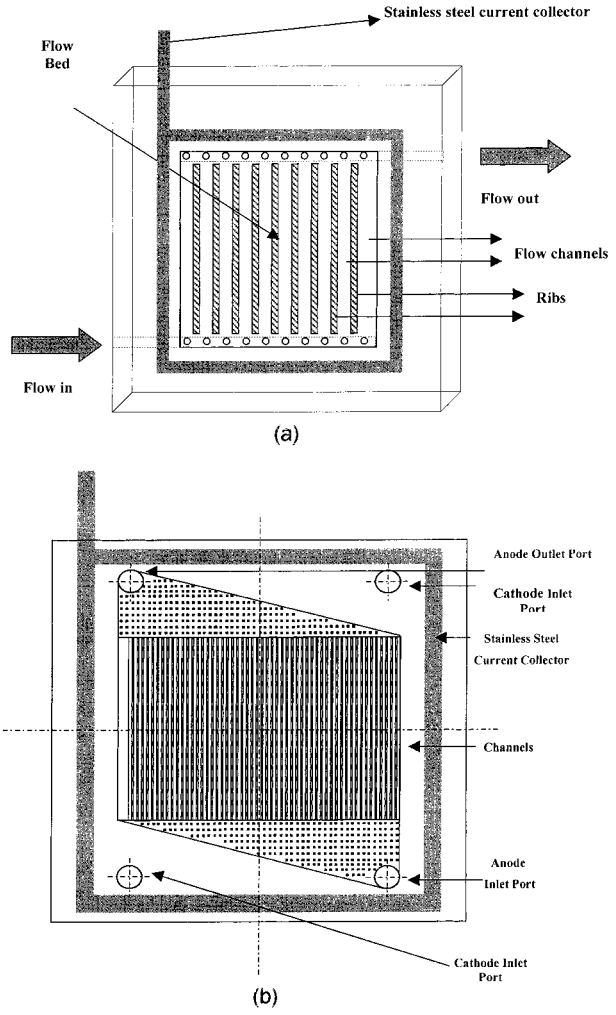

Fig. 2. Flow cell designs. (a) Small cell flow bed design (active area 9 cm^2); (b) Large cell flow bed design (active area 102 cm^2).

The large cell had a different flow bed design to that of the small cell. The design was a result of this research and other research on a large scale DMFC with a flow bed design and manifold arrangement identical to that of the small cell. The design is based on a compact heat exchanger, and is in three sections: a triangular enlarging inlet section, 30 mm long which had a series of 4 mm^2 square spots, a central region of parallel flow channels of the same cross section as the small cell and a triangular, outlet section, of a similar design to the inlet section.

In both cells current was withdrawn using a peripheral stainless steel strip embedded into the acrylic block which contacted the MEA. A limitation with the arrangement is the relatively inefficient way of collecting the current produced (from the periphery with the aid of a stainless steel frame), which limited the cell current density to values below 100 mA cm^{-2} to minimize problems of current maldistribution.

In operation the cells were tested in a simple flow circuit with methanol solution supplied by two Watson Marlow 505U peristaltic pumps. The temperature control was achieved with, a variable voltage supply, an in-house electric heater and a Eurotherm temperature controller with an embedded thermocouple in the methanol solution tank. Air or oxygen gas was supplied from gas cylinders, and the pressure was controlled by a needle valve at the cell cathode side outlet.

The flow of methanol and carbon dioxide gas was recorded using a high speed Hitachi CCTV video camera (HV-720K). A stroboscope was placed behind the camera to provide the necessary lighting for the camera. The images were recorded in a video recorder, and then converted offline to a computer image with the aid of a Matrox PC card. An important issue in designing a DMFC is to ensure that there is a uniform distribution of liquid between all the flow channels, across the cell, to attain a uniform supply of methanol fuel to the MEA. This uniformity of flow was confirmed over a range of flow rates by observing the rise in liquid level in all channels.

3. Results and discussion

An efficient DMFC requires methanol to have access to the anode while the carbon dioxide gas generated is able to freely move away from the catalyst sites on the catalyst surface. The carbon dioxide gas and aqueous methanol solution move counter currently in the catalyst

layer, in the gas-diffusion layer and in the carbon cloth-backing layer. The two phases should ideally flow in discrete paths, rather than as a two phase flow with gas bubbles moving against a liquid flow, induced by the anode reaction and the electro-osmotic transport of water and methanol. To approach this situation the carbon surface is made partially hydrophobic, by adding Teflon, thereby creating regions for free gas movement. In liquid fed DMFCs the issue of gas flow is more critical than in gas/vapour fed cells due to the 'flooded' nature of the anode. The cathode of the DMFC may also be similarly affected by problems of flooding but, in comparison to the anode, this is less critical.

This study was conducted to investigate the mechanism of carbon dioxide gas evolution from the surface of operating MEAs. The supporting materials, either graphite cloth or carbon paper, were treated with Teflon to facilitate gas movement through this layer, whilst ensuring liquid methanol solution entry to the catalyst layer, counter-current to the gas flow.

Figure 3 presents pictures of operating MEAs in both the large cell and small cell with carbon paper or cloth under the same conditions (current density 50 mA cm^{-2}, channel flow rate 2.5 ml min^{-1} per channel). Overall, in the study, we observed that carbon dioxide is not uniformly produced over the surface of the gas diffusion layers, especially in the case of the small cells. A number of point sources of gas release exist, with a continuous high rate bubble generation, and areas with no such activity. This is attributed to the structure of the electrode and the use of Teflon. Tortuous paths that connect the surface with the catalyst area are probably 'flooded' with the liquid phase. Hence, there are a limited number of 'hydrophilic' open channels for carbon dioxide flow. Thus gas could accumulate in the diffusion layer and the reaction layer, and form large bubbles or slugs (compared with the layer structure) which move partly in a vertical plane until they will find an open, horizontal, channel for flow from the reaction site.

As can be seen, from Figure 3, the flow regime is different in the three cases. With carbon paper MEA large gas slugs are formed (0.8–1.8 mm) which attach on the surface of the paper and block the channel. This is explained from the texture of the paper surface (quite rough) which creates a different surface tension between the bubble and the surface and enhances 'friction' between the bubbles, or slugs, and the paper. Hence the gas remains attached to the point of generation and/or accumulation until the buoyancy, or dynamic pressure, force are sufficient to overcome friction and dislodge the bubble/slug. In the long term (typically after a few minutes) this leads to a complete blocking of all the flow bed channels accompanied by a rapid deterioration in the cell electrical performance. This is depicted in Figure 4. Periodically some of the gas is removed, because of the increase in buoyancy forces with increasing gas accumulation, which results in a variation of several millivolt in potential.

With the carbon cloth MEA (Figure 3) the flow regime is bubbly with relatively small gas bubbles (0.6–0.8 mm), which have a tendency to coalesce and form bubble swarms. In addition, since the cloth has a lower 'friction' characteristic, bubbles tend to attach to the acrylic channel walls (the surface is relatively rough due to machining). This feature is beneficial for the DMFC since the surface of the cloth, which is the area for reactant diffusion, is relatively clear and free from

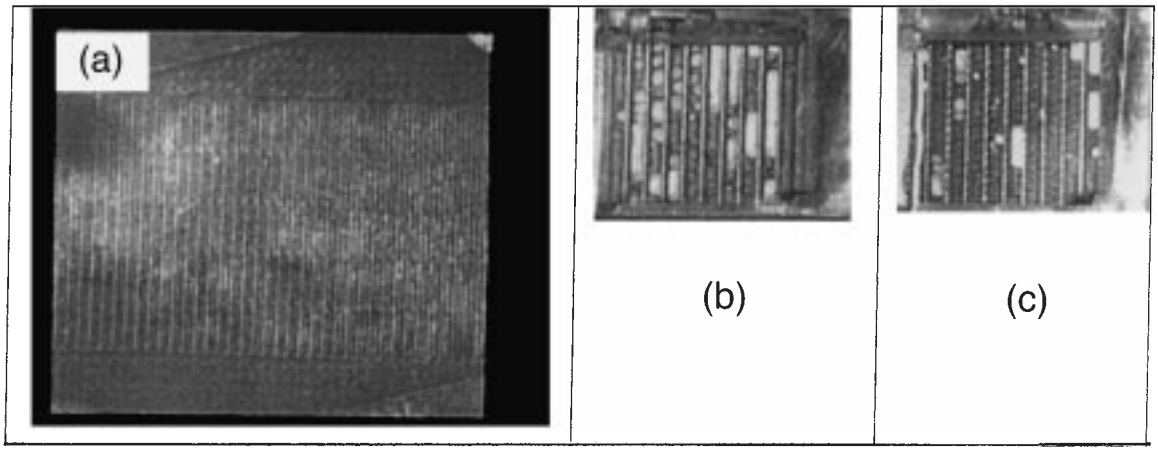

Fig. 3. Gas evolution patterns for the same operating conditions for both cell sizes and for two different gas diffusion backing layer materials. 50 mA cm^{-2}, flow rate 10 cm^3 min^{-1}per channel, 75 °C. Gas evolution for carbon cloth in (a) the large cell and (b) the small cell; (c) gas evolution for carbon cloth in the small cell.

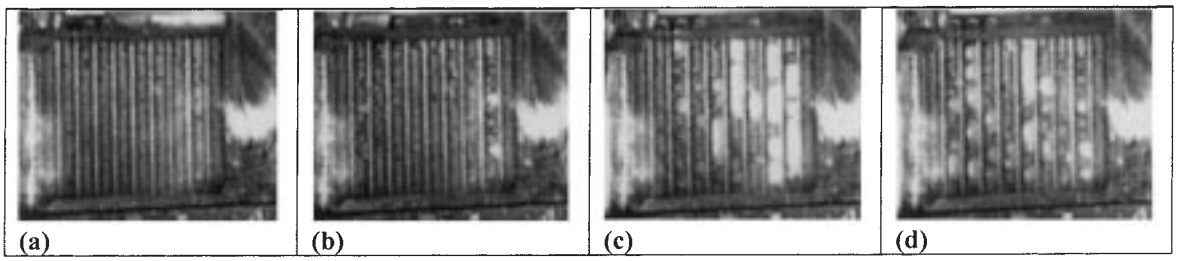

Fig. 4. Dynamic bubble generation behaviour from carbon paper MEA. Conditions: 30 mA cm^{-2}, flow rate 5 cm^3 min^{-1}, 75 °C. (a) 30, (b) 120, (c) 210 and (d) 360 s.

bubbles. This results in superior electrical performance attributable to the enhanced gas management of the cell. In the case of the large cell the bubble flow pattern is even better, with a more uniform flow of bubbles. This is attributed to the better flow manifold design in the larger cell, which is discussed in more detail later. Overall the types of flow observed span the range of fine dispersed bubbles to, large bubbles, to slugs of gas and even to annular flow [10]. The gas generation sites multiplied in all cases: when the current density was increased and when the cathode side pressure was increased.

3.1. *Effect of methanol solution flow rate*

The effect of the anode side liquid phase inlet flow rate was investigated, in both cells and with both materials, in the ranges 5 to 1137 ml min^{-1} for the small cell, and 26 to 1026 ml min^{-1} for the large cell. Figure 5 shows the effect of flow rate, with other conditions the same (current density 30 mA cm^{-2}, 75 °C), for the carbon cloth material in the small cell. It is evident that as the flow rate increases the gas slugs are removed and the bubble size becomes smaller and eventually blocking is virtually eliminated. At the same time, with the increase in liquid flow rate, conditions in the exhaust manifold improve and, at the highest flow rates, no gas slugs are present. The cell voltage response of this cell, shown in Figure 6, indicates the improved performance expected with an increase in flow rate, that is, increase in voltage. Even with the cell used, and low temperatures of operation, there is a performance improvement of some 100 mV over the flow rates used.

Figure 7 shows the effect of flow rate for the case of Toray carbon paper. Again, as with the carbon cloth backing material, increasing the flow rate enhanced gas removal from the flow bed. Generally the behaviour of the carbon paper MEA is similar to that of cloth MEA, except that higher flow rates are required to completely remove the gas slugs. As already mentioned the paper material tended to encourage adherence of gas bubbles to the surface of the material, and consequently over the range of flow rates investigated, total gas slug removal was never achieved. This is evidence that paper material is less satisfactory for use in MEA fabrication.

The manifold design used for the small cell comprised a straight circular cross section tube machined inside the main body of the perspex block, with holes open on its periphery. Each hole had the same diameter as the channel width (2 mm) and was in line with the inlet/outlet of the channel. A problem with the flow distribution design is that the flow changes orientation twice; from vertical upwards to horizontal to enter the internal manifold (placed in 90° inclination from the flow channel), and then horizontally through an angle of 90° to the exit port at the side of the acrylic block. Thus

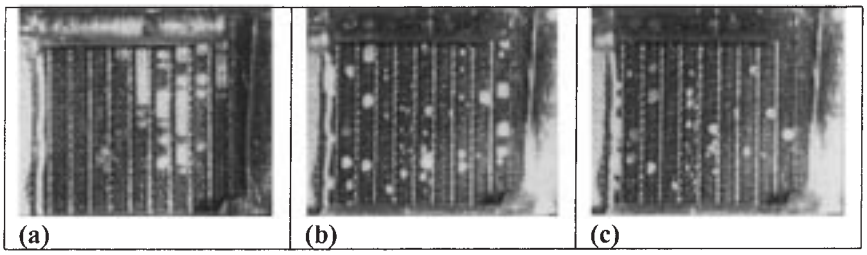

Fig. 5. Effect of anode side liquid phase inlet flow rate on the gas removal characteristics for the small cell with carbon cloth MEA. Conditions: 30 mA cm^{-2}, 75 °C. Flow rates: (a) 10, (b) 413 and (c) 1137 cm^3 min^{-1}.

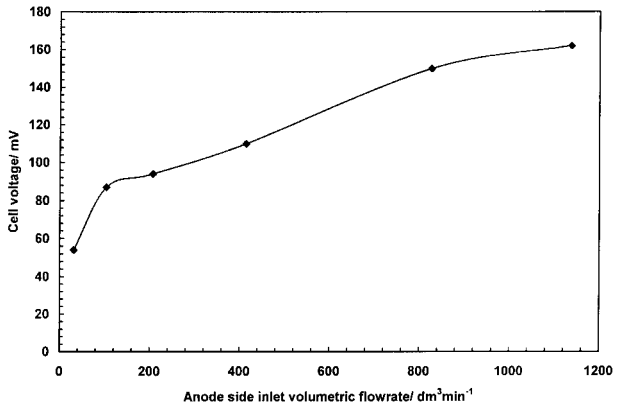

Fig. 6. Cell voltage response of the acrylic flow visualization cell. 75 °C, 30 mA cm^{-2}, carbon cloth MEA.

when gas slugs are produced which have a greater cross section than the hole they must be 'forced' through a hole. This is achieved either by compressing the gas or by breaking the slug into smaller gas bubbles. Both these effects are enhanced by a high liquid phase flow rate, or by an increase in the gas pressure inside the anode side flow bed. In addition the gas flow has to overcome the friction and two-phase flow related pressure drop in the outlet manifold and the exterior flow loop. At low flow rates this is difficult to achieve and only happens when there is an excessive amount of gas trapped inside the cell and the manifold. There are thus instances when all the outlet manifold volume is practically occupied by gas slugs.

The issue of methanol solution flow rate and its effect on cell electrical performance is complicated by the nature of the unusual electrode structure of solid polymer electrolyte cells. The solution flow will influence the cell behaviour through several effects: (i) access of methanol solution into the structure; (ii) removal of carbon dioxide from the active catalyst sites; and (iii) heat exchange between the solution and the catalyst layer.

If the solution temperature is lower than that of the catalyst layer, higher flow rates will encourage greater heat removal from the catalyst causing greater cooling of the catalyst and lower catalyst temperature with thus a reduction in the cell voltage, at a fixed current density. Thus potentially an optimum solution flow rate could exist which gives a maximum in cell voltage performance as the benefits of mass transfer become less significant in comparison to the cooling of the catalyst layer. It is worth noting that frequently temperature 'control' of the cell is by heating pads placed against the outside of the cell and cell temperature is measured in the graphite blocks and not at that actual surface of the catalyst.

The effect of flow rate, over a relatively small range (0.7–2.7 ml min^{-1}), on performance has been examined with several MEAs with different catalyst. Typically, as shown in Figure 8, there is not a significant variation in performance. This data, for 80 °C and 2.0 mol dm^{-3} methanol, suggests that there is no identifiable mass transport limitation for methanol, at this concentration, over the current density range investigated and that there is little influence of carbon dioxide production at the catalyst surface. In this region of flow rates the flow channels contain a significant proportion of carbon dioxide present as slugs. To examine the effect of flow rate further we operated the cell over a much greater range of flow rate and with lower methanol solution concentrations. The latter had the effect of imposing limiting current operation on the fuel cell as is apparent in Figure 9. Measuring the limiting currents, $i_{\lim}$, for the fuel cell we were able to determine the impact of flow rate on cell mass transfer. Figure 10 shows the variation of effective mass transport coefficient with Damköhler number, *Da*, which is a dimensionless group defining the ratio of limiting current density to volumetric flowrate, *Q*,

$$Da = \frac{i_{\lim} A}{6\,F\,C_{\text{methanol}} Q}$$

Here as *Da* increases (i.e., flow rate increases), the mass transport coefficient increases, which corresponds to the

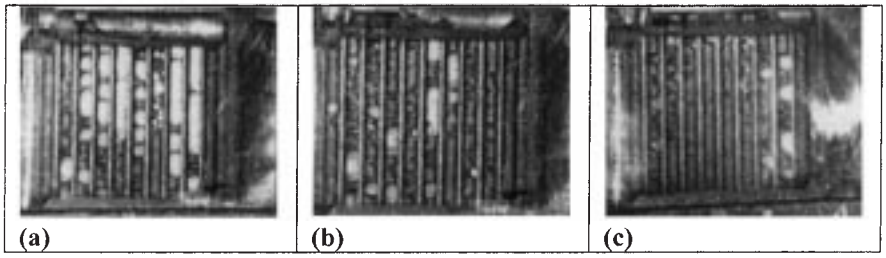

Fig. 7. Effect of anode side liquid phase inlet flow rate on the gas removal characteristics in the small cell for a carbon paper MEA. Conditions: 70 mA cm^{-2}, 75 °C. Flow rates: (a) 5, (b) 413 and (c) 1137 cm^3 min^{-1}.

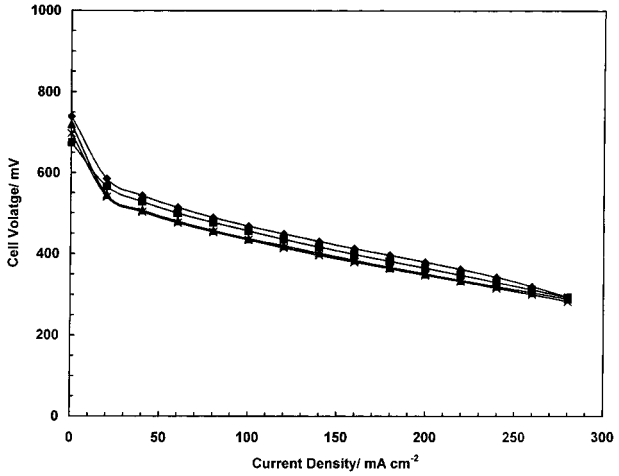

Fig. 8. Effect of flow rate on the cell voltage response of a small DMFC. 2.0 mol dm^{-3}, 90 °C, 2 bar air. Flow rates ◆: 0.84 cm^{-3} min^{-1}, ■: 0.7 cm^{-3} min^{-1}, ▲: 1.4 cm^{-3} min^{-1}, ×: 2.1 cm^{-3} min^{-1}.

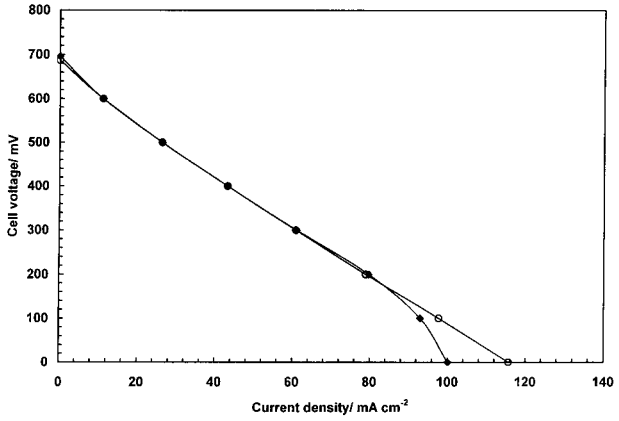

Fig. 9. Effect of flow rate on the cell voltage response of a small DMFC with a low methanol solution concentration. (◆) 4 and (○) 120 cm^3 min^{-1}.

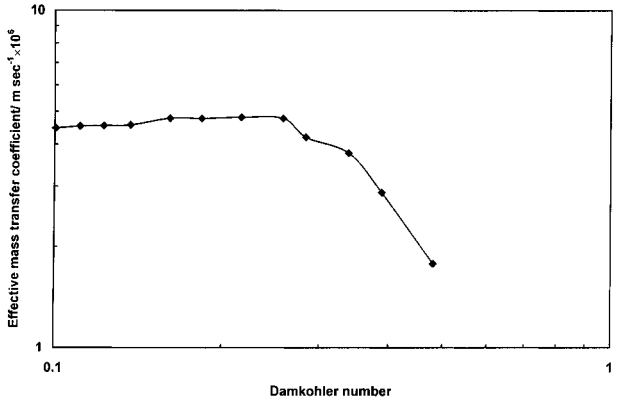

Fig. 10. Effect of Damköhler number on the effective mass transfer coefficient in the DMFC.

anticipated beneficial effect of carbon dioxide removal from the surface of the MEA.

3.2. *Effect of current density*

Figure 11 shows the effect of current density on the gas flow in the small cell with carbon cloth and carbon paper fabricated MEAs, at flow rates of 6 ml min^{-1} and 1137 ml min^{-1}. It is evident that, at both flow rates, the amount of gas present in the flow bed rapidly increases with current density and that for the higher current densities some channels are blocked. Nevertheless the bubble size, the presence of gas slugs and the channel blocking phenomenon are all significantly reduced when higher liquid flow rates are used (Figure 11(b)). It is apparent, in Figure 11(c), that the carbon paper does not provide as good gas removal as the cloth and that almost all the channels are blocked with large slow moving gas slugs. As expected the electrical performance deteriorates with time over a period of a few minutes operation, due to inefficient gas removal.

Figure 12 shows the effect of current density on the gas management in the case of the large cell (liquid flow rate 103 cm^3 min^{-1}, cell temperature 75 °C, 10–50 mA cm^{-2}). As can be seen, there is a gradual increase in the amount of gas bubbles attached to the channels walls. Despite the relatively large amount of gas present, the surface of the cloth is relatively free of bubbles and thus problems of blocking the reactant supply to the catalyst layer seems to be avoided.

4. Conclusions

It is expected that scaling up DMFC will pose significant carbon dioxide removal problems. As the active area increases the amount of gas produced increases significantly. For a large cell of 270 cm^2 (the prototype size to be used in our stack studies) operating at 100 mA cm^{-2} and 1.0 dm^3 min^{-1} liquid flow rate. The gas outlet volumetric flow rate is almost the 40% of the total outlet flow rate. It is a crucial aspect of fuel cell operation, for efficient cell performance, that the channels are relatively clear of gas slugs and are fed continuously with fresh solution. This will secure that the anode side catalyst layer is adequately fed with reactants and that the reaction products will be rapidly removed from the interior of the cell.

The gas evolution and flow patterns observed are significantly different in the small and large cell designs. In the small cell the gas flow is inhibited by the manifold design which cannot accommodate large proportions of gas without experiencing operational problems at low liquid flow rates. The present study showed that a well

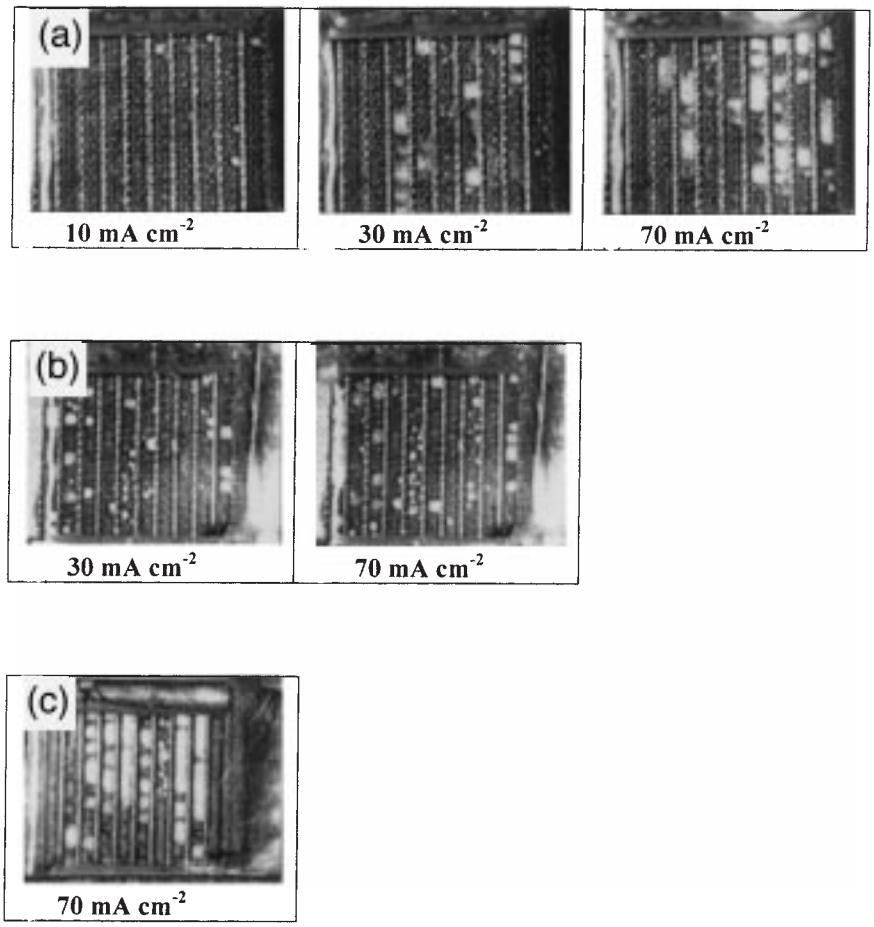

Fig. 11. Effect of current density on the gas removal characteristics for the small cell. 75 °C. Carbon cloth made MEA (a) 6.0 and (b) 1137 cm^3 min^{-1}; (c) carbon paper made MEA at 6.0 cm^3 min^{-1}.

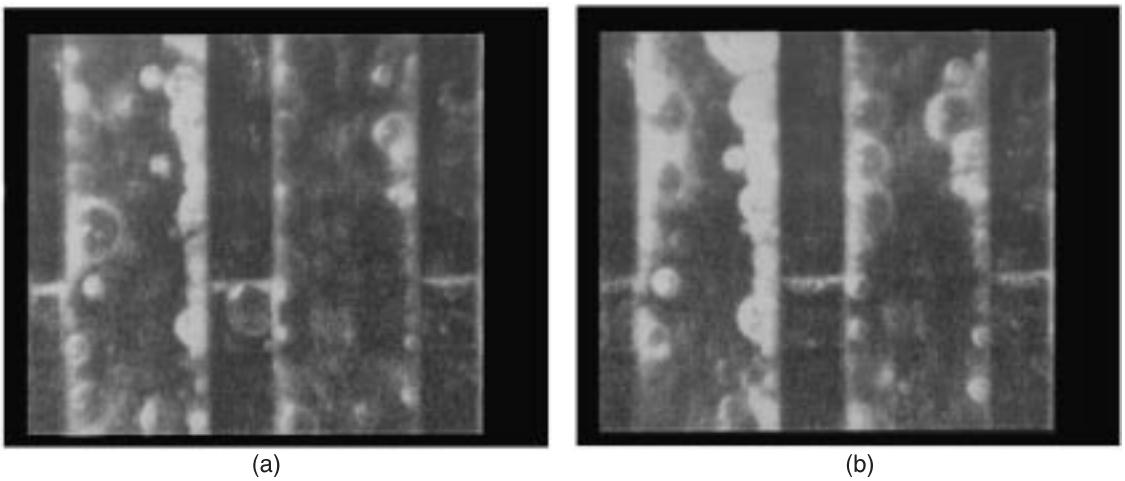

Fig. 12. Effect of current density on the gas removal characteristics for the large cell with a carbon cloth made MEA. 75 °C, 103 cm^3 min^{-1} at current density (a) 10 and (b) 50 mA cm^{-2}.

designed flow bed with a relatively large exit area could be beneficial from a gas management point of view. In the range of parameters investigated in the large cell there was little evidence for the formation of gas slugs even at high current densities: very small, rapid moving gas bubbles are produced.

Acknowledgements

The authors would like to acknowledge the following: the European Commission for supporting P.A. under a TMR Marie Curie research training grant, EPSRC for supporting W.M.T. We also thank Johnson Matthey Technology Centre for supplying catalyst under its loan scheme and K. Sundmacher and S. Kramer for assistance with the mass transport studies.

References

1. K. Scott, W.M. Taama and J. Cruickshank, *J. Power Sources* **65** (1997) 159.
2. S Wainwright, J.T. Weng, R.F. Savinell and M. Litt, *J Electrochem. Soc.* **142** (1995) L121.
3. K. Ravikumar and A.K. Shukla, *J. Electrochemical Soc.* **143** (1996) 2601.
4. S. Surampudi, S.R. Narayanan, E. Vamos, H. Frank, G Halpert, A. LaConti, J. Kosek, G.K. SuryaPakash and G.A. Olah, *J. Power Sources* **47** (1994) 377.
5. T.I. Valdez, S.R. Narayanan, H. Frank and W. Chun, Proceedings of the 12th Annual Battery Conference on Applications and Advances (1997) p. 239.
6. S.R. Narayanan, et al. Proceedings of the Power Sources Conference, Cherry Hill, NJ, USA (1996).
7. K.B. Prater, *J. Power Sources* **51** (1994) 129.
8. A.K. Shukla, P. Christensen A. Hamnett and M. Hogarth, *J. Power Sources* **55** (1995) 87.
9. K. Scott, W.M. Taama and P. Argyropoulos, *J. App. Electrochem.* **28** (1998) 1389.
10. V.P. Carey, 'Liquid–vapour Phase-change Phenomena: An Introduction to the Thermophysics of Vaporisation and Condensation Processes in Heat Transfer Equipment'. (Hemisphere, Washington DC, 1992).
11. P. Argyropoulos, W.M. Taama and K. Scott. 'Engineering and modelling aspects on large scale liquid feed DMFC stacks', 5th Electrochemical Engineering Symposium, Exeter, UK March 25–28 (1999).